5.6.3. DEVICE CHARACTERIZATION

Of the four initial wafers that underwent technological process, only three reached completion, yielding chips as those depicted in Figure 135. Of these, one was a backup wafer in which only the backside polysilicon resistor processes had been carried out, without creating front-side reservoirs, nor undergoing anodic bonding. The goal of including such a simplified wafer was two-fold. On the one hand, the resulting chips were intended for use as clamped drivers/sensors with passive PCR-chips (since they would not present a glass thermal-barrier) and, on the other hand, they were kept as a last resort for polysilicon sensor/actuator characterization in case the complete technological process did not yield the desired results.

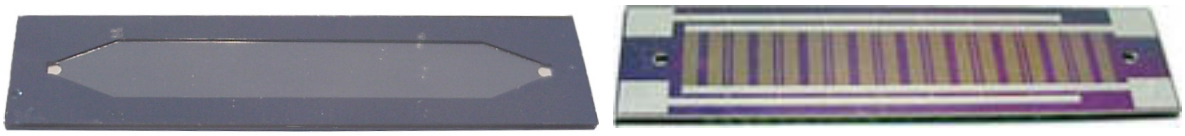

Figure 135 - Front and back views of the fabricated chips.

After fabrication, bonding and cutting of the chips, the fabricated sensor and actuator resistances were characterized with a 86H3 Graphical multi-meter (*Fluke*). Characterization results are charted in Table 19.

Wafer/chip	Actuator R (Ω)	Sensor R (Ω)	Wafer/chip	Actuator R (Ω)	Sensor R (Ω)	Wafer/chip	Actuator R (Ω)	Sensor R (Ω)
AS1	5.8	62.0	BS1	5.5	78.8	C1	6.0	96.1
AS2	5.7	43.8	BS2	5.5	41.1	C2	6.1	97.7
AR1	5.8	41.9	BR1	5.6	83.2	C3	6.1	98.8
AR2	5.8	42.8	BR2	5.9	31.0	C4	6.1	60.8
AR3	5.9	86.5	BR3	5.5	71.2	C5	6.1	97.7
AR4	5.8	47.8	BR4	5.5	47.3	C6	6.1	59.3
AR5	5.7	50.3	BR5	5.5	50.8	C7	5.9	94.7
AR6	5.7	51.6	BR6	5.4	52.6	C8	7.7	91.1
AR7	5.6	54.8	BR7	5.5	77.3	C9	6.2	77.8
AR8	5.5	55.5	BR8	5.5	57.4	C10	5.9	95.7

Table 19 - Actuator and sensor resistance values for normal (A and B) and backup, polysilicon resistor-only (C) wafers. An R denotes rhomboidal chips, while an S denotes serpentine-like chips.

The first fact to be glimpsed from Table 19 is that normal wafers fit reasonably well within expected resistance values (4.28 Ω for actuators and 55.3 Ω for sensors), while the backup wafer (C) shows a larger deviation

from predicted values, an effect that can be readily explained by a somewhat thinner polysilicon layer in wafer C. On the other hand, Table 19 reveals that actuator resistance variance is much lower than that of sensor resistors. Since both devices (sensors and actuators) were created by means of the same polysilicon deposition process, the most feasible hypothesis for this increase in resistance variance must come from the photolithographic process. As mentioned before (see p.236), sensor design implied the outline of polysilicon layers quite close to the resolution limit of the plate-transferred masks here used (see *Materials and Methods*, p.289). Therefore, it is plausible to assume that the variability observed in sensor resistances stems from irregular pattern and non-exact wideness in sensor resistor grid elements.

Still, a more problematic issue was detected in most wafer-A chips. Instead of lying in the whereabouts of MΩ, as it was due to, the cross resistance between sensor and actuator resistors was very low (between 35 and 220 Ω), suggesting that a short-circuit was somehow connecting both kinds of elements. Since sensor and actuator polysilicon grids did not overlap at any point, the only probable hypotheses behind the short-circuit phenomenon were that either aluminum debris (resulting from the last hole-opening deep RIE-etch) was making superficial contact between grids, or else the anodic bonding process had corrupted the intermediate polysilicon-to-aluminum insulating oxide layer and the actuator aluminum tracks (which did overlap with sensor polysilicon layers) were provoking the short-circuit. The first of these hypotheses was partly, although not completely, discarded by immersing one of the short-circuited chips in heated pure 37% HCl solution for 5 s (which should remove any superficial aluminum impurities) and then testing for (and finding) the short-circuit again. When increasing the immersion time to 10 s, the results were inconclusive, since part of the aluminum tracks were degraded in the process. Therefore, it was assumed that the short-circuit came from anodic bonding corruption of the polysilicon-aluminum insulation layer, and that thicker layers should be used in further fabrication processes.

5.6.4. PASSIVE TEST

After electrical characterization, the fabricated devices were functionally tested to assess their feasibility both as PCR vessels, actuators and sensors. This was done in a sequential and incremental manner. First, active chips were tested for PCR-friendliness using them in a passive way, with the

already developed Peltier driving system (see p.173). Once they had passed the passive test, the functionality and performance of chip heaters was assessed, using them as drivers for temperature cycling, while still maintaining a clamped external Pt100 resistor as the controlling temperature sensor. Active chips were then characterized and calibrated as sensors, involving a reconfiguration of the acquisition circuitry, and, lastly, the chips were used as both sensors and actuators without the intervention of external sensing elements to conduct fast PCR amplification.

GCGTCACGGGCTGCTATTGCCAAAGGGTGCGTTGTTGGTGCCGCTGTCATATCAGAGGGTTG
CTCCCATCACTGGCATAGAGTTGTGATGGGGGATGTTTATGTATCGTCAGCACGATGTGCAG
CAGTACTTGAATGCTGTGCTGGATCTGGCTGTATGGGCTTACATGTGCCGCTTGCTAGGGAG
GTTGCTTGTGTCTCTTGTGCTTATTAGTAATAATACTAATT**ATG**AGTTTGAGCGATATTCAGCA
GGCAATCCTGTCATTGATTACCAACAACATCAACGCTGAT***GGCGTTTCTCCTTCGCAGAC***

Figure 136 - Target region of the template DNA, flanked by 19-mer upstream and 20-mer downstream primers (green). The translation start codon for the *lexA* gene is shown in blue, delimiting gene coding (orange) and promoter (grey) regions.

Template validation

After experiencing some problems with the PCR templates previously used (see p.207), it was decided to switch to a new set of template and primers and start from scratch the functional characterization of active PCR-chips. *Xylella fastidiosa* SOS-response regulator *lexA* gene, together with is promoter region, was isolated and cloned into a pGEM-T vector (see *Materials and Methods*, p.321) and, after culture in electro-transformed *E. coli*, the plasmid DNA was extracted and purified. Next, suitable primers for chip PCR were carefully selected using PrimerSelect software (*DNASTAR*®) and acquired from *Sigma-Genosys* (see *Materials and Methods*, p.325). The primers were chosen to enclose a 310 bp fragment of the gene promoter and start regions (see Figure 136), and they were mainly selected to have very similar melting temperatures (ΔTm ~0.3 ºC) and to present low self-priming and primer-dimer formation.

As in previous instances (see p.207), prior to experimentation on PCR-chips, a positive control was run on a conventional thermocycler to assess the validity of the extracted template and of the PCR parameters derived from primer-manufacturer specifications. The PCR and mix protocols are shown in Table 20, while the result of the positive control can be seen in Figure 137.

Quantity	Reagent
17 µl	milliQ H_2O
2.5 µl	10x $MgCl_2$ Buffer
2.5 µl	10 nM dNTPs
1.25 µl	10 µM sense primer
1.25 µl	10 µM antisense primer
0.2 µl	3.5 U/µl Expand™ High Fidelity System (*Boehringer Mannheim Corp.*)
0.3 µl	200 ng/µl sample DNA

Cycling protocol:

95.5 °C - 1 min
95 °C - 5 s \
62 °C - 20 s x40
72 °C - 45 s /
72 °C - 2 min
4 °C - ∞

Table 20 - PCR mix and amplification protocols for the *X. fastidiosa lexA* promoter region amplicate.

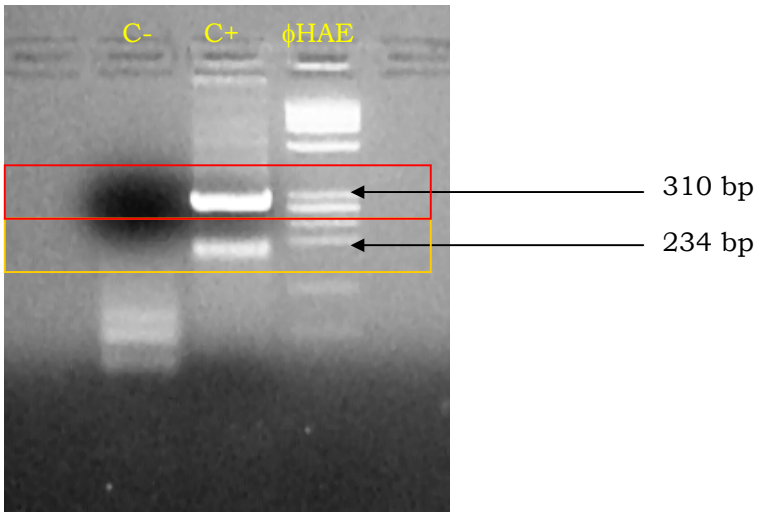

Figure 137 - Negative and positive amplification controls for the above-specified reaction. The use of a ϕHAE ladder (5 µl) in a 3% agarose gel ascertains the validity of the amplified band (red box, ~310 bp) and uncovers a secondary configuration (or primer n-mer structure) below (orange box, ~234 bp).

Chip PCR validation and initial optimization

Chip PCR validation

Having validated the adequacy of the new template stock and PCR protocols, a first tentative assay was carried out with the new active chips, using them in a passive manner with the Peltier driver setup already developed for passive PCR-chips (see p.154). The PCR and mix protocols used in this assay were essentially those of template validation (see Table

20), with the exception that 9.375 µl of BSA were added to the 75 µl master mix (leading to the previously titrated 2.5 µg/µl BSA concentration, see p.200), and that template DNA and Taq concentration were doubled in the chip mix to ensure positive results.

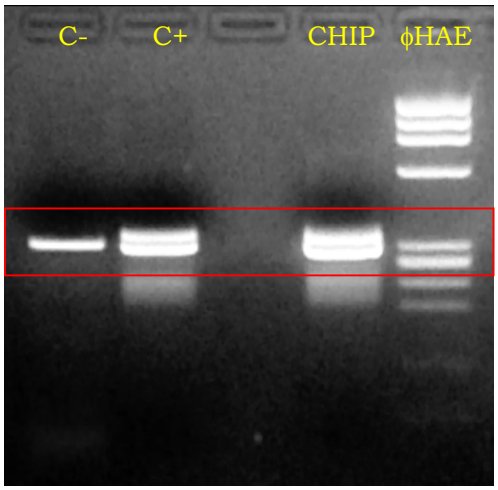

Figure 138 - Positive slab gel (3% agarose, 15 µl per well; 5 µl ϕHAE) results for the chip PCR validation assay using active PCR-chips with the old Peltier drive setup. The negative control reveals contamination possibly due to lack of care in mix elaboration or in gel pipetting. Total chip analysis time: 1:10:10 h.

Initial optimization

After the successful initial chip PCR validation results (see Figure 138), and prior to switching to active chip driving, an initial optimization with the known-to-work Peltier setup was carried out, both to achieve faster reaction times and to minimize the amount of template DNA in chips. The new mix and cycling protocols are shown in Table 21, while slab gel results and cycling performance can be seen in Figure 139.

Quantity	Reagent
17 µl	milliQ H_2O
2.5 µl	10x $MgCl_2$ Buffer
2.5 µl	10 nM dNTPs
1.25 µl	10 µM sense primer
1.25 µl	10 µM antisense primer
0.2 µl	3.5 U/µl Expand™ High Fidelity System (*Boehringer Mannheim Corp.*)
3.125 µl	20 mg/ml BSA
0.3 µl	200 ng/µl sample DNA

Cycling protocol:

95.5 °C - 1 min
95.5 °C - 2 s \
62 °C - 6 s x45
72 °C - 18 s /
72 °C - 1 min
4 °C - ∞

Table 21 - PCR mix and fast cycling optimization parameters. As earlier (see p.210), denaturation times were reduced to spikes (2 s) and annealing and extension times were also reduced (6 s and 18 s), taking into account the high thermal-transfer rate of PCR-

chips. Standard 2.5 μg/μl BSA concentration was maintained and Taq concentration was doubled in the chip mix.

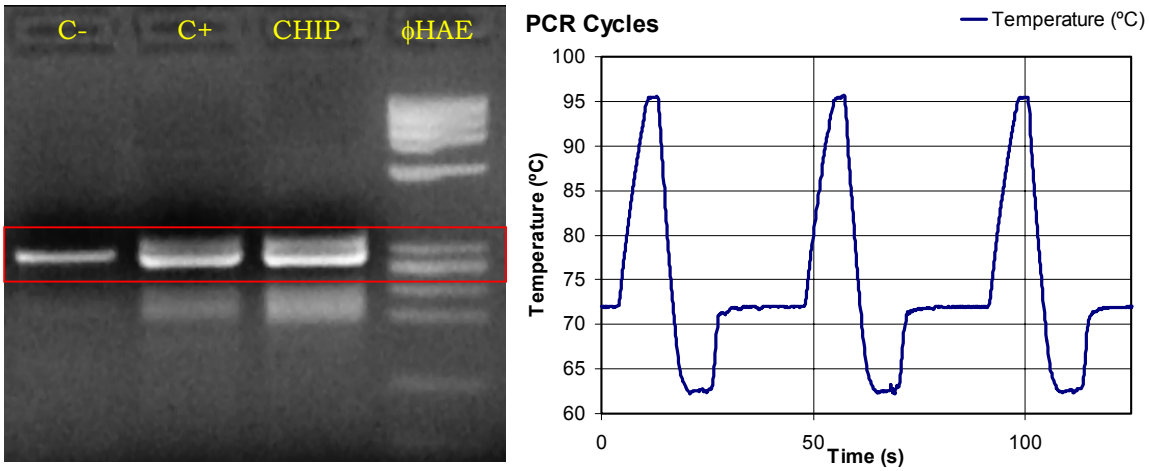

Figure 139 - Slab gel (3% agarose, 20 μl per well; 5 μl for ϕHAE) results and cycling operation for fast PCR reaction with equal amounts of template DNA. The persistence of negative control positives indicates a contamination of reagent stocks, which were subsequently renewed. Total chip analysis time: 33:56 min.

5.6.5. ACTUATOR TEST

Following validation and initial optimization of active chip functional capabilities with the passive Peltier driving setup, the path was set for crosschecking these results using the chip resistors as heat driving mechanisms. At this stage, the goal was to both ascertain the chips heat driving capabilities and their compatibility with PCR (absence of heat non-homogeneities and other possible outcomes of close-grid heating). Therefore, as done previously with polysilicon chips (see p.228), these assays were carried out using the already developed and tested Pt100 sensor and sensing circuitry, and the driving circuitry of Peltier cells. Minimal changes were introduced to the control program (switching to zero drive output, instead of negative output, for cooling), and the PID parameters were optimized for operation on the fast-heating resistors.

Experimental setup

Even though, due to the self-imposed design constrains (see p.234), much of the previously developed apparatus (driving and sensing circuitries, Pt100 sensors, methacrilate insertion/extraction devices) could be readily used in these experiments, a new mechanical assembly was required to establish a common ground for all the ulterior tests with active PCR-chips.

Previous assays with polysilicon chips had relied on the use of dedicated PCB wiring and bonding techniques (see *Materials and Methods*, p.302) or pincer clamping for electrical contact with the chips, but these were clearly not feasible alternatives for conducting repetitive experiments with active PCR-chips. On the one hand, and having the electrical contacts at the same face as the access ports, the use of PCB dedicated wiring techniques posed strong hindrances onto chip sealing and, moreover, it precluded chip reuse, since mounted chips would be difficult to cleanse and, certainly, could not undergo autoclave sterilization processes (see *Materials and Methods*, p.316). On the other hand, relying on pincer clamping for electrical contact also introduced some serious problems for chip sealing, while still not providing a solid ground for reproducible experimentation (fixed fan location, airtight sealing or stable electrical contacts).

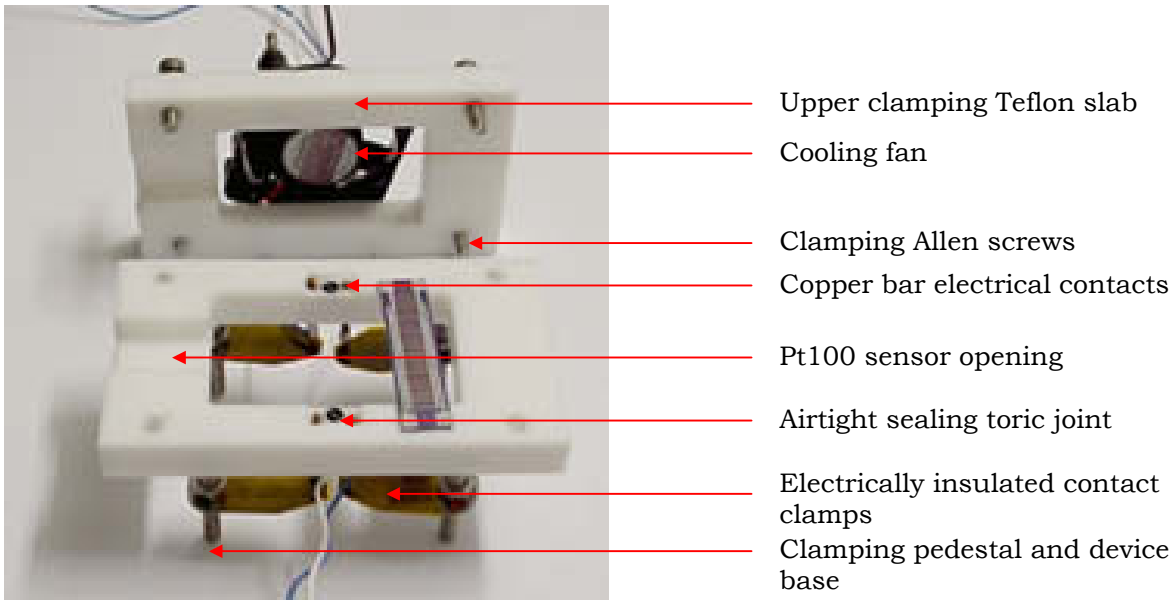

Figure 140 - Tailored Teflon devices for integrated active chips test. Four electrical ports (two for sensing and two for drive) are provided by pedestal-clamped Ø1 mm copper bars. Typical operation was as follows: the chip was first mounted (face down) onto the toric joints and screw-clamped to provide airtight sealing. Thereafter, copper bars were put into place and clamped until reliable electrical contact was achieved.

The solution to this conundrum was the development of novel, custom-devised mechanical devices that could both hold the chip in place, provide airtight sealing and offer solid and stable electrical contacts. Previously developed Teflon devices for small Peltier cell operation (see p.181) were retrofitted to accommodate electrical access holes, copper bar pedestal-

clamped contacts, an attached cooling fan and a large opening for Pt100 sensor introduction (see *Materials and Methods*, p.300 for details). The completed devices (see Figure 140) offered effective airtight sealing through toric joints, together with reliable and steady electrical connections, and were used in all subsequent experimentation with active PCR chips.

Functional test

After development and test of the new experimental setup, experiments were carried out to functionally validate the behavior of polysilicon resistors as heat drivers. The previously optimized (see Table 21, p.244) PCR mix and cycling protocols were used here again, and tested against rhomboidal and serpentine-like PCR-chips. The outcome of these assays and the thermal behavior of resistor heat cycling are documented in Figure 141.

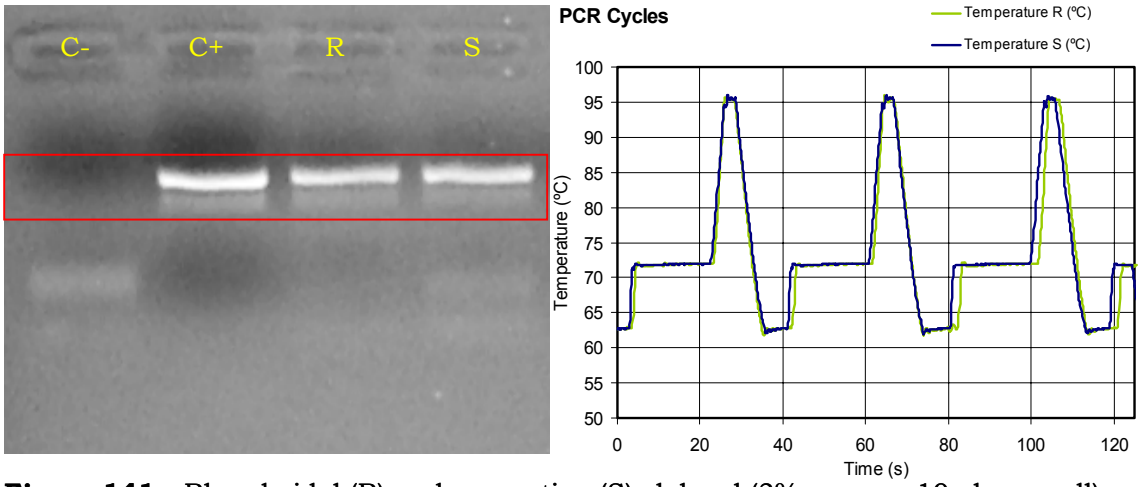

Figure 141 - Rhomboidal (R) and serpentine (S) slab gel (3% agarose,10 µl per well) results give no evidence of significantly different yields. Average heating rate: 8.9 °C/s. Average cooling rate: 4.8 °C. Mean power consumption: 3.37W. Mean analysis time: 31:20 min. Chips used: BS1, BR2.

As it can be seen in Figure 141, positive results were obtained for both rhomboidal and serpentine-like chips, showing no clear-cut evidence of significantly different yields between these schemes (a fact not previously contrasted in the literature). Analysis times were slightly superior to those of Peltier-driven assays, although the full capabilities of polysilicon-driven systems were not be exploited here, since drive was limited to 15W for control reasons and the placement of the Pt100 sensor interfered substantially with the fan-driven cooling airflow. Nonetheless, these positive results proved the validity of active polysilicon resistor grid heating and paved the way for the more elaborate step of calibrating and using

polysilicon temperature sensors as the sole temperature control mechanism in fully independent active PCR-chips. This was an important step, since, coupled with the here-reported use of compatible CMOS technology, it could lead the path towards fully integrated, batch-fabricated and independently programmable PCR-chips.

5.6.6. SENSOR-ACTUATOR TEST

Acquisition circuitry redesign

Theoretically, since both kinds of resistors had a similar (50-100 Ω) resistance, the existing Pt100 conditioning circuitry (see p.157) could have been used for polysilicon resistor data acquisition. Nevertheless, reusing the Pt100 circuitry meant that reliable Pt100 data would not be available during polysilicon sensor calibration and initial operation, and it was deemed safer to keep the Pt100 input operational until polysilicon resistors had been completely calibrated and tested. Therefore, new circuitry had to be implemented for 4-wire resistor reading of the polysilicon resistors and the PC data acquisition board had to be reconfigured in NRSE (non-referenced single ended) mode to allow more analog inputs. Consequently, the whole "bridge" circuit containing the Pt100 signal conditioning circuitry was redesigned to fit a 4-wire polysilicon resistor sensing mechanism and to adapt grounded signals for NRSE data acquisition mode. To make the extra circuitry fit into the RF-blocking box, minimize the number of PC-DAC inputs to be used and speed-up software conditioning, a somewhat different 4-wire sensing circuitry was used here for Pt100 and polysilicon resistor monitoring.

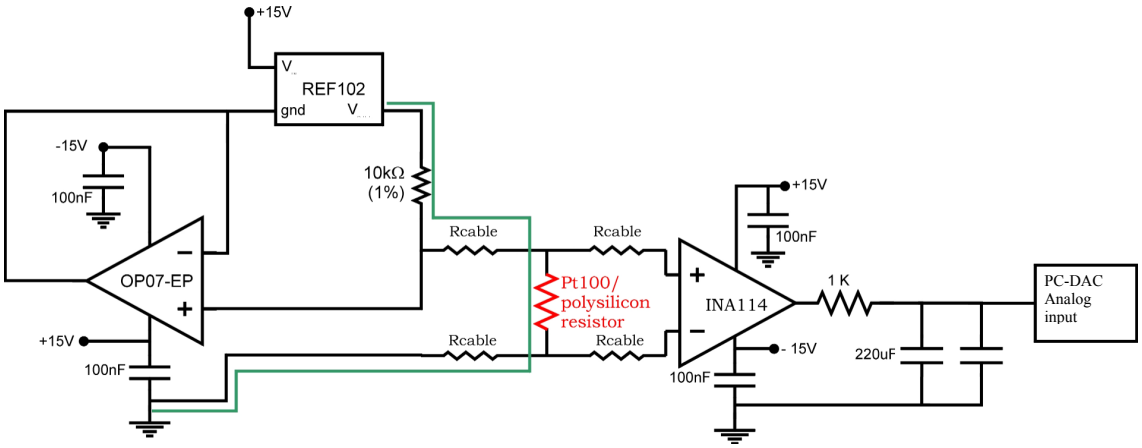

Figure 142 - Redesigned Pt100/polysilicon resistor sensing circuitry. The shown schematic was duplicated for Pt100 and polysilicon resistor signal conditioning.